Assessing Performance of Silicon Photonic Modulators for Pulse Amplitude Modulation

Hassan Sepehrian, Amin Yekani, Wei Shi, and Leslie A. Rusch

IEEE Journal of Selected Topics in Quantum Electronics, (Volume 24, Issue 6) (2018)

Doi: 10.1109/JSTQE.2018.2854607

https://ieeexplore-ieee-org.acces.bibl.ulaval.ca/document/8410444/

Assessing Performance of Silicon Photonic Modulators for Pulse Amplitude Modulation

Hassan Sepehrian, Amin Yekani, *Student Member, IEEE*, Wei Shi, *Member, IEEE* and Leslie A. Rusch, *Fellow, IEEE*

Abstract— Silicon photonic (SiP) electro-optic modulators are key component in cost-efficient and integrated optical transmitters. Modulator design traditionally use figure of merits (FOMs) that characterize modulation efficiency and propagation loss of light, which underestimate the modulator-induced power penalty due to intersymbol interference, as they do not consider the electro-optic bandwidth limitation. We show that in presence of limited electro-optic bandwidth of SiP modulator, the conventional FOMs, such as $V_\pi L$ and $V_\pi \alpha L$, are unable to predict the minimum transmitter power penalty (TPP). Normalized optical modulation amplitude (OMA_N) is proved through simulation to be a reliable tool to predict the minimal TPP point. Then, we introduce a new figure of merit that includes not only the efficiency of the modulator, but also the bandwidth limitation from SiP electro-optic modulator. The new FOM that is derived from OMA_N, translates the system-level requirements of a PAM-*M* optical link to the device-level design parameters. This FOM can be hired to optimize driving voltage swing, bias voltage, and phase-shifter length or to simply choose a SiP modulator with minimal imposed TPP.

***Index Terms*—Bandwidth limitation, depletion mode modulator, figure of merit, link penalty, silicon photonic, normalized OMA.**

I. Introduction

SILICON photonics (SiP) is a promising solution for the next generation of integrated optical transceivers, from optical interconnect in short reach application to medium reach and even long-haul optical links. They are of interest as they can be integrated on complementary metal-oxide semiconductor (CMOS) platforms [1]. The combination of SiP electro-optic devices and CMOS integrated circuits, via monolithic or hybrid integration, paves the way for highly integrated CMOS-photonic solutions for optical transmission links [2-5].

The electro-optic modulator is a crucial component in an optical transmission link. SiP modulators have been widely examined as a cost-efficient, integrated solution [6-11]. In particular, Mach-Zehnder modulators (TW-MZM) are among the most popular for commercial optical transmitters due to their thermal insensitivity, simple driving configuration, and high tolerance to fabrication imperfections. Several high performances SiP TW-MZM are reported [9-11]. Although these modulators have achieved low bit error rates (BERs) at high symbol rates, they have not necessarily achieved optimal designs for a given system context. To design an optimized electro-optic modulator, specific system-level criteria and performance quality factors have to be considered. These factors could be different for an integrated optical modulator compare to its stand-alone discreet counterpart.

Traditionally, TW-MZMs were implemented in non-silicon based electro-optic platforms (i.e., $LiNbO_3$), benefiting from the inherent electro-optic effect of the material. TW-MZM for these low-loss optical platforms have performance determined by two parameters (assuming matched impedance): the required voltage to generate π radian phase shift, known as V_π, and the electro-optic bandwidth. The electro-optic effect has an almost linear relation between the phase variation and the applied driving voltage. The efficiency, defined as $V_\pi L$, is employed to quantify the modulation performance. The bandwidth optimization and efficiency could be decoupled in this design, and V_π is in general independent of bias voltage in $LiNbO_3$.

Although $V_\pi L$ clearly shows the trade-off between the modulator length and the required voltage for π radian phase shift, it does not include the optical loss introduced by the phase shifter. This becomes crucial in the case of silicon modulator due to the significant optical absorption in p-n doped silicon waveguides. More recently $V_\pi \alpha L$ (known as efficiency-loss) is used to quantify SiP modulation performance, where α parameterizes optical propagation loss induced by the silicon waveguide phase shifter [12-13].

However, neither $V_\pi L$ nor $V_\pi \alpha L$ is able to truthfully reflect the system-level performance of the modulator in a real optical link. This limitation can be attributed to the absence of the modulator electro-optic bandwidth in the FOM. Moreover, in contrast to $LiNbO_3$, V_π of the electro-optic modulators in silicon is not a linear function of the applied voltage [14] nor *L*. Hence, the values of $V_\pi L$ and $V_\pi \alpha L$ of a SiP modulator change with its length and bias voltage.

A new figure of merit (FOM) of SiP modulators was presented recently for on-off keying (OKK) [15], which takes into account system parameters such as peak-to-peak drive voltage, bit rate, modulator rise-fall time, and optical modulation amplitude. A low pass filter parameterized by the rise-fall time was employed to capture bandwidth limitations. It was suggested that the measured rise-fall time could be modified to account for PAM-M signaling.

In this work, we examine the transmission power penalty (TPP) induced by the SiP modulator to study the system-level performance degradation caused by SiP modulator in an unamplified optical pulse-amplitude-modulation (PAM) link for short-reach applications such as data centers. The SiP

Manuscript submitted 1 February 2018. This work was supported by Huawei Canada and NSERC (CRDPJ 486716-15).

Authors are with Department of Electrical and Computer Engineering, Centre for Optics, Photonics and Lasers (COPL), Université Laval, Quebec G1V 0A6 Canada (e-mail: Hassan.sepehrian.1@ulaval.ca).

National Science and Engineering Research Council of Canada (NSERC) Funding: CRDPJ 486716-15

modulator limiting factors (optical loss, limited extinction ratio and electro-optic bandwidth limitation) are included in the TPP. A normalized optical modulation amplitude (OMA_N) is shown via simulation to be a reliable predictor of the minimal achievable TPP. Based on these insights, a new FOM is presented that includes not only the optical loss and efficiency, but also the SiP modulator electro-optic modulation bandwidth, BW_{EO}. In contrast to [15], this new FOM does not require parameters extracted from the large-signal analysis. Our simulation shows that it can well reflect the impact of the modulator on OMA and TPP. In addition, the use of BW_{EO} rather than the rise-fall time is more convenient as a modulator is typically characterized by its bandwidth in comparison to the operating baud rate. This new FOM can map SiP modulator physical design parameters to its system-level performance, facilitating both device design and system optimization.

This paper is organized as follows. In Section II we describe SiP TW-MZM simulation. Section III presents the definition of the dynamic TPP including the BW_{EO} limitation. In section IV, OMA_N is presented and employed to define a new figure of merit (FOM). Various simulations are presented to demonstrate the utility of the FOM. Finally, a summary of achievements in this work is presented in section V.

II. SiP TW-MZM Modeling

A. *SiP modulator model and operation*

Consider a typical TW SiP Mach-Zehnder modulator that employs silicon waveguides with lateral p-n junctions. Fig. 1a presents a schematic of a SiP TW-MZM driven in a series push-pull configuration. A negative voltage is applied between the two arms of the MZM, and the traveling wave electrodes are terminated through a matched load.

The cross section of the SiP TW-MZM in a CMOS compatible SiP process on a 220-nm SOI wafer with 2 µm buried oxide (BOX) and lateral p-n junction (i.e., A∗STAR's IME, Singapore) is illustrated in Fig. 1b. To reduce the series resistance without significantly increasing optical propagation loss, intermediate P+ and N+ doping levels are used. Highly doped P++ and N++ regions are used for ohmic contacts. A slow-wave electrode with a T-shaped extension is used for velocity matching between the optical and RF signals [10].

The design in Fig. 1a is simulated in Lumerical Mode software. We use lateral pn junction doping densities of NA=5×10^{17} cm^{-3} and ND=3×10^{17} cm^{-3} and a wavelength of λ = 1550nm, unless otherwise noted. We find the change in effective index, Δn_{eff}, in Lumerical as a function of applied reverse voltage. A plot of Δn_{eff} is given in Fig. 1c.

Let V_{in} be the RF input voltage that can be positive or negative and falls between $-V_{\text{pp}}/2$ and $V_{\text{pp}}/2$. The input voltage in combination with a bias voltage V_{b} is applied in the push-pull configuration seen in Fig. 1a. Due to the inductive bias coupling, one arm sees RF voltage V_{b} plus $V_{\text{in}}/2$, while the other arm sees V_{b} minus $V_{\text{in}}/2$. The inset in Fig. 1a shows two types of input voltage V_{in}: a sinusoidal input and a PAM4 signal. In push-pull operation and assuming two identical arms for the TW-MZM, the instantaneous modulator phase shift is given by

$$\Delta\varphi\left(V_{in}\right)=\left[\Delta n_{eff}\left(V_b+\frac{V_{in}}{2}\right)-\Delta n_{eff}\left(V_b-\frac{V_{in}}{2}\right)\right]\frac{2\pi L}{\lambda} \quad (1)$$

The instantaneous output power is given by

$$P_{out}=P_{in}e^{-\alpha L}\cos^2\left(\Delta\varphi\left(V_{in}\right)/2+\theta_0\right) \quad (2)$$

The phase offset between the two arms is nominally set at $\theta_0=\pi/4$, but can be tuned to any value by use of an on-chip heater. This default choice sets operation at quadrature. For zero input voltage, the output is at its median value (cosine squared is one-half). For an effective index change that is linear in applied voltage, at quadrature the output power is symmetric (vis-à-vis input voltage) about this median, and we can get maximum output swing.

B. *Effect of nonlinear Δn_{eff} on push-pull operation*

The input voltage swing to achieve an output swing from maximum to minimum of the cosine-squared function is called V_π. For effective index change that is linear in applied voltage (such as lithium niobate) we have

$$\Delta n_{eff}\left(V_{in}\right)=V\cdot m\ \Rightarrow P_{out}\propto\cos^2\left(\frac{\pi L}{\lambda}mV_{in}+\frac{\pi}{4}\right) \quad (3)$$

In this case $V_\pi=\lambda/2Lm$, which is independent of bias voltage.

For nonlinear effective index change, however, each bias voltage yields a different V_π. To find this value we define V_{x} as the voltage (a negative value) that achieves maximum cosine squared for a given V_{b}, and V_{y} as the voltage (a positive value) that achieves minimum cosine squared. They solve

$$\begin{aligned}\Delta n_{eff}\left(V_b+V_x/2\right)-\Delta n_{eff}\left(V_b-V_x/2\right)&=-\lambda/4L\\ \Delta n_{eff}\left(V_b+V_y/2\right)-\Delta n_{eff}\left(V_b+V_y/2\right)&=+\lambda/4L\\ V_\pi&=V_y-V_x\end{aligned} \quad (4)$$

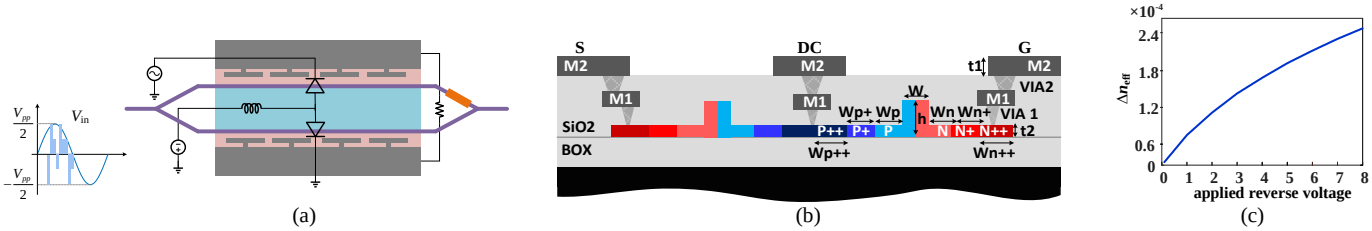

Fig. 1. a) Traveling wave electrode MZM in series push-pull driving scheme; b) cross section of lateral P-N junction waveguide Wp++ = 5.2, Wp+ = 0.83, Wp = 0.37, Wn++ = 5.2, Wn+ = 0.81, Wn = 0.39, W = 0.5, h= 0.22, t1 = 2, t2 = 0.9 (all the dimensions are in µm). c) Δn_{eff} vs. applied reverse voltage for (b).

National Science and Engineering Research Council of Canada (NSERC) Funding: CRDPJ 486716-15

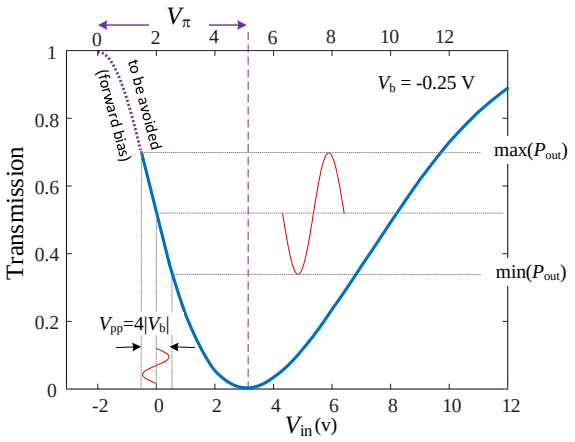

Fig. 2. For the SiP MZM in Fig. 1, operating at quadrature: instantaneous output power for length L =5 mm for V_b=-0.25 V.

The case for λ = 1550 nm, L = 5 mm, V_b = -0.25 V is given in Fig. 2 as a plot of transmission (normalized output power) vs. input voltage. In general, the definition of V_π may encompass a voltage input range that is not desirable for all bias voltages. For instance, V_y may be larger than $|V_b|$, leading to forward bias operation. Forward bias is to be avoided for wide bandwidth operation. In a push-pull driving scheme where the RF input voltage is split in half, the bias voltage should be at least as negative as $V_{pp}/4$. For maximum swing when operating at quadrature we choose $V_{pp} = 4|V_b|$.

Unlike $LiNbO_3$, each V_b generates a different power curve, and a different V_π. In the balance of the paper, all values of V_π are found using the nonlinear Δn_{eff} behavior found in Lumerical simulations of a specific phase shifter length L, and numerically solving (2) given the bias V_b being investigated.

III. TPP INCLUDING ISI

A figure of merit is only as good at the TPP from which it is developed. We start this section with expanding the static ER-limited TPP (see Appendix A) to accommodate the modulator limited bandwidth. Then we discuss the impact of the bandwidth limitation on the total TPP.

A. TTP due to limited electro-optic bandwidth

The bandwidth limitation of a modulator increases the link penalty by introducing intersymbol interference (ISI). ISI is often the ultimate limit to achievable bit rate in high performance systems. Hence, it is critical that the TPP encompass this limitation.

Focusing on PAM-M modulation, we further develop an estimate of the ISI penalty under several simplifying assumptions. Fig. 4 gives an illustration of a typical PAM-4 eye diagram; the eye is noiseless and eye closing is strictly due to the finite rise and fall times. If the modulator had infinite bandwidth, the eye would be rectangular with eye opening equal to the distance between rails, as indicated in Fig. 3. The presence of a limited bandwidth, BW_{EO}, leads to the eye becoming less open. We define the ISI penalty, Δ_{ISI}, as the

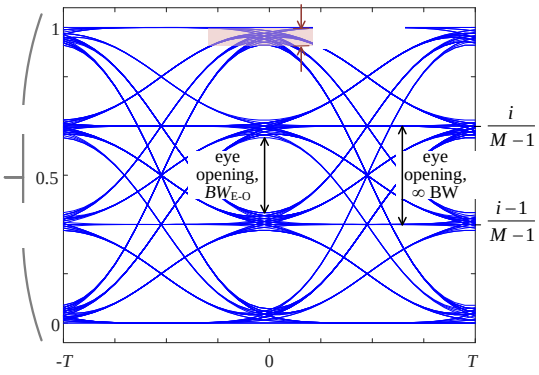

Fig. 3. Noiseless eye diagram for PAM-4 modulation format; Gaussian shaped pulses with BW_{EO}/BR = 0.9.

difference between the infinite bandwidth eye opening and the limited bandwidth eye opening. Note that to the right of the eye diagram we have labeled levels for arbitrary M levels of modulation.

We adopt the simplifying assumptions proposed in [16]. The first simplifying assumption in finding the ISI penalty is the pulse at the modulator output having a Gaussian shape that is parameterized by BW_{EO}. The eye diagram in Fig. 3 was plotted for this Gaussian pulse shape for BW_{EO} = 18 GHz and BR = 20 Gbaud. The next simplifying assumption is ISI dominated by contributions from the two nearest neighbors; contributions from more distant symbols are neglected. Finally, we find the decrease in the eye opening on the upper most eye, as illustrated in Fig. 3, and use it as the nominal ISI penalty. This simplification provides a tractable closed-form solution.

Recall that the term $P_{ER(PAM)}$ already accounts for multiple PAM eyes across a reduced extinction ratio. Under the assumptions described, the ISI leads to an additional power penalty in dB of

$$P_{ISI} = 10\log_{10}\left(1 - M\cdot\mathrm{erfc}\left(\frac{\pi}{2\sqrt{\ln 2}}\frac{BW_{E-O}}{BR}\right)\right) \qquad (5)$$

where erfc is the complementary error function. Details of the derivation are provided in appendix B. We define the total or dynamic TPP that includes effect of modulator bandwidth limitations

$$TPP = P_{\alpha\cdot L} + P_{\mathrm{ER(PAM)}} + P_{ISI} \qquad (6)$$

Note that the signal may also suffer from distortions due to modulator nonlinearity (small in push-pull operation near the linear operating region of the MZ transfer function) or fabrication errors. These issues can be addressed through design of driving circuits and improvement of the fabrication process. Here we focus on understanding of the fundamental limitations in TPP and design optimization of the modulator.

B. Impact of bandwidth limitation on TPP

When the optical loss and limited extinction ratio are the only shortcomings of the modulator, higher extinction ratio leads to a lower static TPP, as seen in Fig. 4b. For a fixed value of RF driving voltage (V_{pp}), increasing the phase-shifter length

National Science and Engineering Research Council of Canada (NSERC) Funding: CRDPJ 486716-15

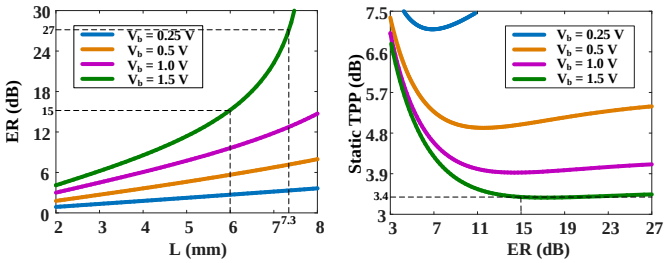

(a) (b)

Fig. 4. For PAM-4 modulation of SiP MZM in Fig. 1, operating at quadrature at various bias voltages with V_{pp}=4|V_b| a) ER vs. phase modulator length L, and b) transmitter power penalty (TPP) vs. extinction ratio. Fig. 4b takes these ERs and calculates the TPP (i.e., for PAM-M, $P_{ER(PAM)}$ replacing P_{ER} in (16). We can see that ER increases as the modulator length; however, the static TPP shows a minimum for a given bias due to the increased loss.

improves the extinction ratio (by decreasing the V_π), as seen in Fig. 4a. There is some downside to the move to longer phase shifters; higher optical loss eventually overshadows ER advantages, i.e., higher extinction ratio will not always improve the static TPP. However, the static TPP vs. L has a very shallow bowl shape for long L. We see from Fig. 4b that bias voltage affects the shallowness of the bowl shape in SiP, as bias voltage affects V_π.

Consider now the dynamic TPP (6) that takes into account the bandwidth limitation of the modulator. In Fig. 5, we plot in pink dashed line (y-axis on the right) the dependence of this bandwidth, BW_{EO}, on L. All other plots in Fig. 5 refer to the y-axis to the left. The static TPP is also included for easy reference in the dashed black curve. The bandwidth is calculated using Lumerical software. Here we have assumed perfect impedance matching of 50 Ω and no velocity mismatch between RF and optical signals. This can be achieved by a proper electrode design [10,18]. The bandwidth of the modulator is then dominated by the RF loss along the electrode loaded by the pn-junction [18].

The dynamic TPPs (6) is shown in solid lines for several baud rates. We report multiple baud rates, as it is the ratio of bandwidth to baud rate, implicit in (5) that determines the relative importance of the ISI contribution to TPP in(6). At 14 Gbaud, the ratio BW_{EO}/BR is large for almost all L (see pink curve); therefore, ISI is negligible at 14 Gbaud. At this low baud rate, the static TPP and dynamic TPP nearly coincide (green, solid 14 Gbaud and black, dashed static TPP). This is to be expected, as (6) collapses to (16) for low ISI.

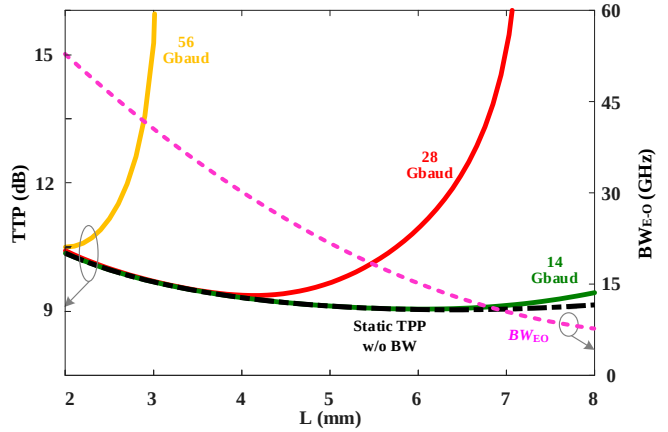

Fig. 5. New TPP from(6), with y-axis at left, for different baud rates (solid lines) when V_{pp} = 4|V_b |= 3V; black dashed line is static TPP without bandwidth effects; pink dotted line is electro-optic bandwidth BW_{EO}.as a function of L when V_b=*-0.75*, with y-axis at right.

Most modern communications systems are designed to push the baud rate to achieve maximal throughput for the network. We can see that as baud rates become more aggressive, the dynamic TPP has a much steeper bowl shape than the static TPP. Hence, at these rates the static TPP is a poor guide to the best choice of phase shifter length. While the static TPP has a minimum in the region of 6-7 mm for the phase shifter, the new TPP tells us this value is only valid for low baud rates. At rates as high as 56 Gbaud, the minimum penalty is found at L = 2 mm. Even at 28 Gbaud, the optimal L is around 4.5 mm, far from the value predicted by the old TPP.

The traditional FOMs ($V_\pi L$ and $V_\pi \alpha L$) have been based on minimizing the static TPP (See appendix A). These FOMs focused on behavior in Fig. 4a, improving ER and optical loss by targeting a wide eye opening without ISI. From our examination of the dynamic TPP, this approach will not guide the designer to an optimal choice of L. It cannot truthfully predict the system level performance for SiP as they overlook bandwidth constraints. In $LiNbO_3$ modulators, bandwidth could be addressed without affecting efficiency. For SiP, bandwidth and efficiency performance measures are intricately intertwined. In the next section, we find a strategy to find an FOM that can nonetheless account for ISI.

IV. TPP AND FOM

Being now armed with an improved TPP that tracks the impact of a given design (phase shifter length L), and operating point (driving voltage and baud rate), we go in search of a useful figure of merit to optimize performance. We consider a normalized optical modulation amplitude as a good predictor of performance, and propose a FOM inspired by this quantity.

A. *Normalized optical modulation amplitude*

Consider optical modulation amplitude (*OMA*) for a potential FOM. Higher *OMA* corresponds to more open optical eye, thus lower BER and consequently, lower TPP. With an interest in PAM-M modulation, we consider the following normalized version of the *OMA*.

$$OMA_N = \frac{1}{M-1}\left(\frac{\max\limits_{\{\text{open eye}\}} P_{out} - \min\limits_{\{\text{open eye}\}} P_{out}}{P_{in}V_{pp}}\right) \qquad (7)$$

This approach focuses on extinction ratio in the PAM-M eyes and removes the dependence on input power and driving voltage. We compare via simulation the behavior of the dynamic TPP and the normalized OMA_N for several baud rates. It is important to note that the output power extrema are defined over an open eye.

We generate pseudo-random PAM-4 data at each baud rate. The square wave signals are passed through a low pass filter with a Gaussian shaped frequency response with a 3-dB

National Science and Engineering Research Council of Canada (NSERC) Funding: CRDPJ 486716-15

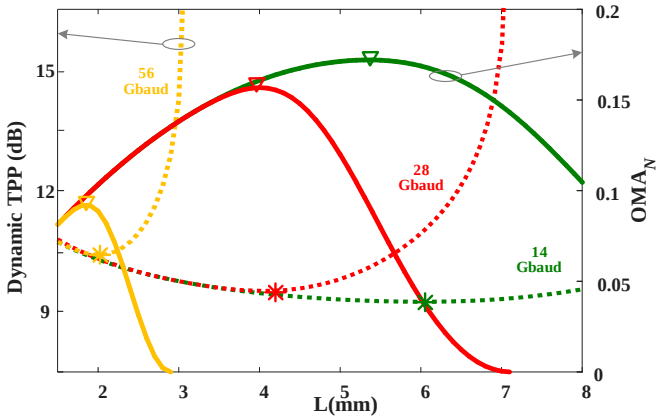

BR (Gbaud)	14	28	56
ΔTPP (dB)	0.03	0.03	0.1
ΔL (mm)	0.55	0.25	0.25

Fig. 6. Dynamic TPP (with bandwidth limitation) and normalize OAM for different baud rates when $V_{pp} = 4|V_b| = 3$V; triangles indicate maxima of FOM, while asterisks indicate minima of TPP. Deviations in phase shifter length L at these extrema, and excess penalty are given in the table.

bandwidth equal to BW_{EO} for the given modulator design (fabrication process and phase shifter length L) and operating point ($V_{pp} = 4|V_b|$). The filtered waveform is used to calculate the output power via (2) using Δn_{eff} found numerically for the given design. The maximum and minimum output power over an open eye are used in (7) to find OMA_N.

We simulated three baud rates, *BR*: 14, 28 and 56 Gbaud for PAM-4 modulation. In Fig. 6, we recreate in dotted lines the dynamic TPP from Fig. 6 for each *BR*, referring to the left y-axis. The OMA_N (right y-axis) is presented in solid lines. We see that the OMA_N has inverse behavior to the TPP. An asterisk indicates the minimum values of the TPP, while triangle markers indicate the maxima of OMA_N, that is,

$$L_{OMA} = \min_L OMA_N \quad L_{TPP} = \min_L TPP \qquad \text{(asterisks)} \qquad \text{(triangles)} \tag{8}$$

Let ΔL to be the difference between the true optimal L (minimum TPP) and the optimal L predicted by the OMA_N.

$$\Delta L = L_{OMA} - L_{TPP} \tag{9}$$

Let ΔTPP be the excess penalty of the best choice for L predicted by OMA_N, and the best choice of L predicted by the minimum TPP, i.e.

$$\Delta TPP = TPP\left(L_{OMA}\right) - TPP\left(L_{TPP}\right) \tag{10}$$

This is the excess TPP when using the OMA to design the phase modulator. Both ΔTPP and ΔL are given in the table below Fig. 6. We can see that the deviation and the excess penalty are small. Hence, normalized OMA can be used as a measure to predict an optimum modulator design for a given system operating driving voltage V_{pp} (or equivalently, bias point V_b).

B. Figure of merit with bandwidth limitation

We begin with the normalized OMA in (7) and strive to reduce the terms to retain the essence of the dynamic TPP behavior, while highlighting the parameters wielding the greatest influence. We start with a discussion of how OAM_N could resemble previous FOMs, and how the bandwidth limitation manifested itself in OAM_N. .

Suppose the modulator transfer function and Δn_{eff} are linear in applied voltage. In this case, the maximum modulator swing, the highest PAM value less the lowest PAM value yields (see appendix C):

$$\max_V P_{out} - \min_V P_{out} \propto P_{in} e^{-\alpha L} \frac{V_{pp}}{V_\pi} \tag{11}$$

Under this assumption, (7) becomes

$$OMA_N \propto \frac{1}{M-1}\frac{1}{P_{in}V_{pp}}\frac{P_{in}e^{-\alpha L}V_{pp}}{V_\pi} = \frac{1}{M-1}\frac{1}{e^{\alpha L}V_\pi} \tag{12}$$

This only brings us to a denominator $e^{\alpha L}V_\pi$, where α represents the optical loss per unit length of the modulator. Assuming a Taylor expansion for the exponential in total loss (small αL), this yields the previous efficiency-loss FOM, $V_\pi \alpha L$.

We are missing the low-pass filtering present in the simulated OMA_N. The efficiency-loss FOM is applicable to a DC input, or an infinite bandwidth response to a data modulated signal. The steepness in the inverted bowl of the OMA_N can be attributed to the ISI-induced reduction in the eye opening illustrated in Fig. 4, which is modeled mathematically by the low-pass Gaussian filter in the simulation (see appendix C). Therefore, assuming a linear response of output power in the applied voltage range, we use the Gaussian filter employed in the dynamic TPP to introduce an ISI term with (12) and define the new FOM as

$$\frac{1}{OMA_N} \propto FOM = V_\pi \alpha L \frac{M-1}{1 - M \cdot \mathrm{erfc}\left(\frac{\pi}{2\sqrt{\ln 2}}\frac{BW_{EO}}{BR}\right)} \tag{13}$$

Note that BW_{EO} is a function of L and V_b. As discussed in appendix B, the complementary error function can be well approximated by an exponential in the region of BW_{EO}/BR observed in typical optical communications systems. This approximation leads to

$$FOM = V_\pi \alpha L \frac{M-1}{1 - \frac{M}{2}\exp\left(-4.34\left(BW_{EO}/BR\right)^2\right)} \tag{14}$$

where *BR* is the system baud rate, BW_{EO} is the modulator 3-dB bandwidth and M is the PAM modulation level. The V_π term is found as described in (4), and is a function of the system operating driving voltage, V_{pp} (or equivalently bias point V_b) and the modulator length, L. Hence the FOM is a function of the fabrication process (parameters used in Lumerical to find Δn_{eff}), the operating point (baud rate and driving voltage), and the phase shifter design (L which determines BW_{EO}).

In Fig. 7, we simulate four baud rates for PAM-4 modulation format. The FOM (right y-axis) is presented in solid lines. For convenience, here and in the following calculations, we use values of α in dB/cm and thus the FOM is in V·dB. We see that the FOM has the same steep bowl behavior observed in the TPP. Stars are used to indicate minima of FOM, while diamonds

National Science and Engineering Research Council of Canada (NSERC) Funding: CRDPJ 486716-15

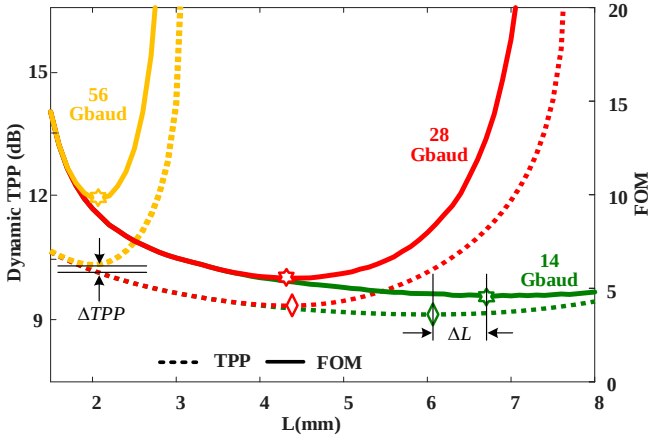

BR (Gbaud)	14	28	56
ΔTPP (dB)	0.03	0.03	0.1
ΔL (mm)	0.6	0.15	0.2

Fig. 7. Dynamic TPP (with bandwidth limitation) and new FOM for different baud rates when $V_{pp} = 4|V_b| = 3$V; stars indicate minima of FOM, while diamonds indicate minima of dynamic TPP. Deviations in phase shifter length L at these minima, and excess penalty are given in the table.

indicate minima of dynamic TPP. The excess dynamic TPP, ΔTPP, and ΔL the deviation in the FOM predicted optimal L and TPP predicted optimal L are reported in the table below the figure.

We readily observe that the FOM has achieved our objectives: it is an excellent predictor of optimal design with only minimal excess penalty, and 2) it is a simple function of system parameters both readily simulated and readily characterized experimentally.

Previous results were limited to one choice of bias voltage and four baud rates. We simulated the excess TPP when sweeping both bias voltage (or equivalently driving voltage since we assume $V_{pp} = 4|V_b|$) and baud rate. Results are presented in Fig. 8 as a color map. We observe that the excess TPP remains below 0.1 dB for the entire range of operating points and system baud rates. Indeed, the majority of the examined space has excess TPP below 0.05 dB.

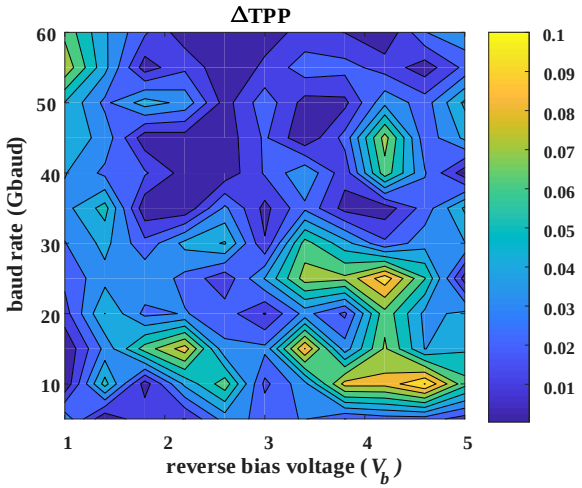

Fig. 8. Excess TPP in dB when using optimal L found from FOM, L_{FOM} rather than optimum L found from TPP directly, L_{TPP}.

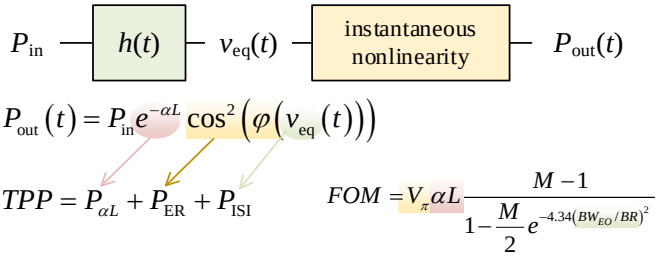

Fig. 9. Mapping of impairments to their representations in the transmission power penalty and the FOM.

C. Discussion

We pause here to make a few observations about the FOM that has been developed. The mathematical model we assumed had two important characteristics, as illustrated in the block diagram of Fig. 9. We model the modulator as having a low pass impulse response following a Gaussian shape parameterized by a 3-dB bandwidth. The filtered signal is then assumed to experience an instantaneous nonlinearity described by the raised cosine function. In addition, there is the loss proportional to phase shifter length in the modulator.

Compared to the FOM in [15], we both use a low pass filter whose shape is parameterized by a ratio capturing the relative importance of the bandwidth limitation: in our case $BW_{E\text{-}O}/BR$, in their case the ratio of rise time to bit duration. In [15], the order of the low pass filter was assigned by fitting measured data for binary NRZ; here, we used a theoretical approach. This allowed us to relate the low pass filter bandwidth to the phase shifter length L, as detailed in the appendix B. Next, a Gaussian shape filter is used to yield a closed form expression for the filtering effect (via the erfc). For this reason, our FOM has an exponential dependence on $BW_{E\text{-}O}/BR$. Note that by basing our filter on phase shifter length, our FOM can be used directly for TW-SiP ZM design.

The low pass nature of the model captures the ISI produced by a limited bandwidth modulator. ISI appears in the TPP in the form of a power penalty due to decreased eye opening. ISI appears in the FOM in a simplified expression for that decreased eye. We note that our model ignores the instantaneous nonlinearity in the calculation of the decreased eye, i.e., that the low pass occurs before the cosine squared. We call this nonlinearity instantaneous because it assumes infinite bandwidth, that is, any change in input voltage is immediately observed as a change in output power. The true modulator may be a non-instantaneous, non-stationary nonlinearity.

The V_π term is deceptively simple. We must not forget that in SiP V_π depends on the bias voltage as well as L. As previously discussed in section II, the SiP FOMs cannot assume a constant product $V_\pi L$, as is found in lithium niobate modulators. For an existing modulator, V_π can be readily measured; in developing a design it can be simulated by combining information on Δn_{eff} in Lumerical and information on the driving voltage.

We have focused on improving the sub-eye opening in PAM-M modulation format, not just the outer eye. By contrast, [15] focused on the overall extinction ratio (i.e., outer eye). That FOM has to be adjusted (through modification of the bit interval

National Science and Engineering Research Council of Canada (NSERC) Funding: CRDPJ 486716-15

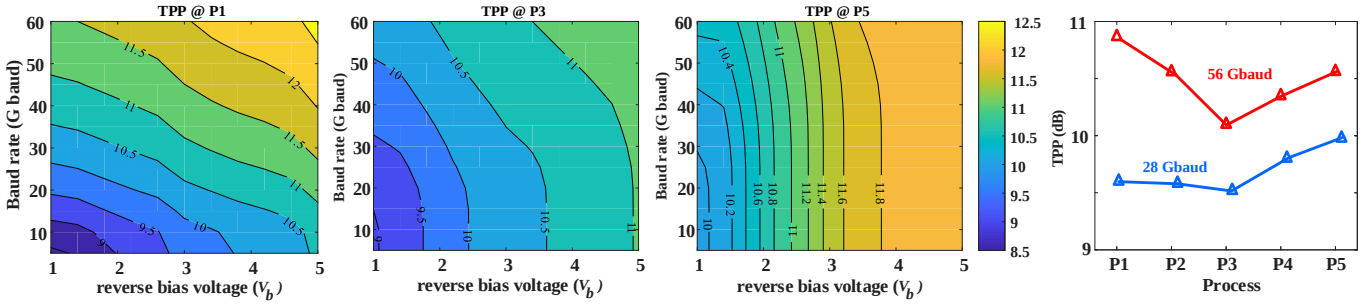

Fig. 10. All simulations are PAM-4 modulation of a modulator operating at quadrature. The excess TPP as a function of reverse bias and baud rate are given for doping concentrations of a) -50%, b) 0%, c) +50%; d) Effect of different doping concentration on excess TPP for two different baud rates at $V_{pp} = 4|V_b| = 2$ V.

and the low pass filter order) for different modulation formats. The dependence on system and MZM parameters is directly visible in our FOM.

D. FOM for different doping concentration

In order to examine how the optimum point predicted by the new FOM changes when the process parameters change, we simulate FOM for a SiP TW-MZM in a lateral p-n junction process (see Fig. 1b) with five distinct doping concentrations. In this set of simulations, we consider *P3* (used to produce results throughout the paper, including Fig. 8) as a reference process, where doping densities are $NA = 5\times10^{17}$ cm^{-3} and $ND = 3\times10^{17}$ cm^{-3}. *P1*, *P2*, *P4*, and *P5* are processes whose doping concentrations compared to *P3* are modified by -50%, -25%, +25%, and +50%, respectively.

We have already established in Fig. 8 that the excess TPP is small for P3. Although not presented here, simulations for the other processes yielded similar results; the excess was small. Therefore, in this section we present instead the absolute TPP performance for different process choices.

We plot the minimum TPP (by sweeping the phase shifter length) in dB for different baud rates and bias voltages for *P1*, *P3* and *P5*. In Fig. 10a, 10b and 10c, respectively. When the doping concentration is relatively low, *P1* case, the low efficiency of the phase shifter is the dominant limiting factor. A longer phase shifter is needed to achieve same TPP as *P3*. However, longer phase shifter will affect BW_{EO}. This effect could be observed in Fig. 10a, where compare to *P3* in Fig. 10b, minimum TPP is more sensitive to the baud rate.

On the other hand, when the doping concentration is increased compared to *P3*, optical loss is the main limiting factor. To achieve the same TPP as *P3*, a shorter phase shifter is needed, translating into higher BW_{EO}. Fig. 10c shows that TPP is very sensitive to the reverse bias voltage that increases the optical loss, but less sensitive to the baud rate.

While these previous figures allow us to find performance for any operating point for three of the potential fabrication processes, suppose the operating point is fixed and we wish to compare processes directly. We select $V_{pp} = 4|V_b| = 2$ V for two transmission rates, 56 Gbaud and 28 Gbaud PAM-4. We plot the TPP versus the five potential fabrication processes in Fig. 10d. For either baud rate, P3 is the best trade-off, although the difference is marked at 56 Gbaud, and less critical at 28 Gbaud. This plot shows how the new FOM can be used to select a process according to system level requirements.

V. Conclusion

A simple closed-form expression is provided for a figure of merit (FOM) to assess SiP TW-MZM modulator performance in an optical pulse-amplitude-modulation (PAM) link. The FOM is a function of modulator parameters that can be easily found either via simulation (during the design process) or characterization (in selecting an appropriate, existing modulator). Unlike the proposed one, traditionally used FOMs ($V_\pi L$ and $V_\pi \alpha L$) are unable to predict the effect of limited bandwidth in SiP modulators.

Extensive simulations validated the efficacy of the FOM to predict system performance as quantified by the transmission power penalty (TPP). The new FOM maps the physical and design parameters of a SiP TW-MZM to its system-level effect in a PAM-*M* optical link. One can use this FOM to choose the optimum bias and driving voltage, or optimally design a modulator for specific system-level criteria. The FOM allows us to observe how far the baud rate could be pushed for a tolerable range of TPP. Finally, the effect of variation in process is also presented, confirming that the new FOM not only can be used to predict the optimum phase-shifter length, bias voltage or driving signal in a specific process, but also to select the optimum doping concentration to minimize the SiP TW-MZM TPP for a given system context.

Although we have focused on TW-MZMs, the methodology and optimization procedures described in paper could be extended and be applied to other modulators as well.

Appendix

A. Static TPP for OOK

Previous efforts to develop a figure of merit for silicon photonic modulators have by in large focused on on-off keying (OOK). In order to obtain the maximum optical eye opening, the modulator is operated at its quadrature point. The output excursions for this configuration result in a certain extinction ratio (ER) and optical modulation amplitude (OMA) defined as

$$ER = \frac{\max P_{\text{out}}}{\min P_{\text{out}}} \quad OMA = \max P_{\text{out}} - \min P_{\text{out}} \qquad (15)$$

National Science and Engineering Research Council of Canada (NSERC) Funding: CRDPJ 486716-15

Previous transmitter power penalty (static TPP) considers a reduction in output power due to loss and limited extinction ratio [17]

$$TPP_{\text{static}} = P_{\alpha L} + P_{ER} \tag{16}$$

The first term, $P_{\alpha L}$ reflects the optical loss introduced by the phase-shifter. The second term, P_{ER}, accounts for reduced extinction ratio for a fixed driving voltage swing due to high V_π, without considering the bandwidth limitation. For OOK, the penalty from limited extinction ratio is defined as the increase in average power needed to obtain the same bit error rate as an ideal pulse with infinite extinction ratio.

For a multilevel modulation format (e.g., PAM-*M*) the received optical power must be split among *M* symbols. For simplicity, we consider a short-research link without optical amplification. Assuming that thermal noise dominates the receiver noise and that equal separation between PAM levels [4], the power penalty from limited ER for PAM-*M* is

$$\begin{aligned} P_{ER(PAM)} &= P_{ER(\text{OOK})} - 10\cdot\log_{10}\left(\frac{M-1}{\log_2 M}\right) \\ &= 10\cdot\log_{10}\left(\frac{ER-1}{ER+1}\times\frac{\log_2 M}{M-1}\right) \end{aligned} \tag{17}$$

where ER is in dB.

B. ISI effect with Gaussian response

1) TPP ISI term

As mentioned in section IIB, limited electro-optic bandwidth induces ISI. To facilitate calculations, we assume the pulse shape is Gaussian, the output of a filter with impulse response

$$h(t) = \frac{1}{\sigma\sqrt{2\pi}} e^{-t^2/2\sigma^2} \tag{18}$$

As the Fourier transform of a Gaussian is also Gaussian, the transfer function of this filter is also Gaussian. The 3-dB bandwidth of the filter determines the parameter σ. Fig. 3 illustrates the eye diagram of the output of such a filter for a typical case - a ratio of 0.9 of bandwidth ($BW_{\text{E-O}}$) to baud rate (*BR*). The input is a sequence of rectangular pulses spaced at $T = 1/BR$ seconds. We can see there are *M*-1 eyes, each diminished by a somewhat different value of intersymbol interference. Our goal is to determine a simple expression for the decrease in eye opening due to a limited bandwidth filter.

We use the approximations suggested in [15]. We neglect ISI from distant pulses, and consider only the contribution for the time adjacent input rectangular pulses. We find the worst case (top of upper-most eye), Δ_{ISI}, calculated for this simple case. With no bandwidth constraint, a middle eye would have opening of 1/(*M*-1). We assume the worst case ISI level is present at each symbol transition. This leads to an average ISI level on a given eye of

$$\begin{aligned} \frac{M}{M-1}\Delta_{\text{ISI}} &= \frac{M}{M-1}\text{erfc}\left(\frac{T/2}{\sigma\sqrt{2}}\right) \\ &= \frac{M}{M-1}\text{erfc}\left(\frac{\pi}{2\sqrt{\ln 2}}\frac{BW_{E-O}}{BR}\right) \end{aligned} \tag{19}$$

where erfc is the complementary error function (the result of the convolution of a rectangular pulse of width *T* with the Gaussian impulse response with variance σ). The ISI penalty can be found from the ratio of eye opening for limited bandwidth to eye opening with infinite bandwidth. Hence

$$\begin{aligned} &10\log_{10}\left(\left[\frac{1}{M-1} - \frac{M}{M-1}\text{erfc}\left(\frac{\pi}{2\sqrt{\ln 2}}\frac{BW_{E-O}}{BR}\right)\right]\Big/\frac{1}{M-1}\right) \\ &= 10\log_{10}\left(1 - M\cdot\text{erfc}\left(\frac{\pi}{2\sqrt{\ln 2}}\frac{BW_{E-O}}{BR}\right)\right) \end{aligned} \tag{20}$$

is used in our TPP to represent the ISI penalty, P_{ISI}.

2) FOM ISI term

The erfc can be well approximated by an exponential over a limited range of the argument. The majority of optical communications systems would have $BW_{\text{E-O}}/BR$ in the range of 0.4 to 2. A larger number would be under utilizing the available bandwidth resource, while a smaller number would have too high an ISI penalty. In this range

$$\begin{aligned} \frac{M}{M-1}\text{erfc}\left(\frac{\pi}{2\sqrt{\ln 2}}\frac{BW_{EO}}{BR}\right) &\cong \frac{M}{M-1}0.506e^{-4.34(BW_{EO}/BR)^2} \\ &\cong \frac{M}{M-1}\frac{1}{2}e^{-4.34(BW_{EO}/BR)^2} \end{aligned} \tag{21}$$

This gives a good approximation of the decrease in PAM-M eye opening due to the presence of ISI. The ISI penalty can be found from the ratio of eye opening for limited bandwidth to eye opening with infinite bandwidth. Hence the ratio of eye opening for limited bandwidth to eye opening with infinite bandwidth is

$$\begin{aligned} &\left[\frac{1}{M-1} - \frac{M}{M-1}\frac{1}{2}e^{-4.34(BW_{EO}/BR)^2}\right]\Big/\frac{1}{M-1} \\ &= 1 - \frac{M}{2}e^{-4.34(BW_{EO}/BR)^2} \end{aligned} \tag{22}$$

and is used in our FOM to represent the ISI penalty.

C. Linear assumption of the maximum output swing

Considering a linear assumption for the transmission of the MZI and variation of Δn_{eff} versus voltage in the swing range of the driving voltage (V_{pp}), the numerator in (11) can be simplified as:

$$\left(\max P_{out} - \min P_{out}\right) \propto P_{in}e^{-\alpha L}k\times V_{p-p} \tag{23}$$

where *k* is the slope of the transmission curve in Fig. 2 at quadrature point and is proportional to *L* and $\partial(\Delta n_{eff}) / \partial(\text{V})$. Assuming a linear variation of Δn_{eff} versus applied reverse voltage (blue curve in Fig. 1.c):

$$\frac{\partial \Delta n_{eff}}{\partial V} = m \Rightarrow k \propto m\times L \tag{24}$$

where *m* is a constant. In addition, for a specific *L*:

$$\begin{aligned} \pi &= \frac{2\times\pi\times\Delta n_{eff}(V_\pi)\times L}{\lambda} \\ \Rightarrow \frac{2\times m\times V_\pi\times L}{\lambda} &= 1 \Rightarrow L \propto \frac{1}{mV_\pi} \end{aligned} \tag{25}$$

National Science and Engineering Research Council of Canada (NSERC) Funding: CRDPJ 486716-15

From (23) to (25), $k \sim m/V_\pi$, hence:

$$\max P_{out} - \min P_{out} \propto P_{in} e^{-\alpha L} \frac{V_{pp}}{V_\pi} \tag{26}$$

ACKNOWLEDGMENT

We thank Dr. Zhuhong Zhang and his team with Huawei Canada for useful discussions. This work was supported by Huawei Canada and NSERC (CRDPJ 486716-15).

REFERENCES

[1] P. Dong, X. Liu, S. Chandrasekhar, L. L. Buhl, R. Aroca and Y. K. Chen, "Monolithic Silicon Photonic Integrated Circuits for Compact 100^+ Gb/s Coherent Optical Receivers and Transmitters," in *IEEE Journal of Selected Topics in Quantum Electronics*, vol. 20, no. 4, pp. 150-157, July-Aug. 2014.

[2] H. Sepehrian, A. Yekani, L. A. Rusch and W. Shi, "CMOS-Photonics Codesign of an Integrated DAC-Less PAM-4 Silicon Photonic Transmitter," in *IEEE Transactions on Circuits and Systems I: Regular Papers*, vol. 63, no. 12, pp. 2158-2168, Dec. 2016.

[3] X. Wu *et al*., "A 20Gb/s NRZ/PAM-4 1V transmitter in 40nm CMOS driving a Si-photonic modulator in 0.13µm CMOS," *2013 IEEE International Solid-State Circuits Conference Digest of Technical Papers*, San Francisco, CA, 2013, pp. 128-129.

[4] Chi Xiong, Douglas M. Gill, Jonathan E. Proesel, Jason S. Orcutt, Wilfried Haensch, and William M. J. Green, "Monolithic 56 Gb/s silicon photonic pulse-amplitude modulation transmitter," *Optica 3*, 1060-1065, 2016.

[5] M. Cignoli *et al*., "22.9 A 1310nm 3D-integrated silicon photonics Mach-Zehnder-based transmitter with 275mW multistage CMOS driver achieving 6dB extinction ratio at 25Gb/s," *2015 IEEE International Solid-State Circuits Conference - (ISSCC) Digest of Technical Papers*, San Francisco, CA, 2015, pp. 1-3.

[6] C. Li *et al*., "Silicon Photonic Transceiver Circuits With Microring Resonator Bias-Based Wavelength Stabilization in 65 nm CMOS," in *IEEE Journal of Solid-State Circuits*, vol. 49, no. 6, pp. 1419-1436, June 2014

[7] Y. Hsu *et al*., "64-Gbit/s PAM-4 20-km transmission using silicon micro-ring modulator for optical access networks," *2017 Optical Fiber Communications Conference and Exhibition (OFC)*, Los Angeles, CA, 2017, pp. 1-3.

[8] R. Dubé-Demers *et al*., "Ultrafast pulse-amplitude modulation with a femtojoule silicon photonic modulator," *Optica* ***3***, 622-627 (2016).

[9] A. Samani *et al*., "A Low-Voltage 35-GHz Silicon Photonic Modulator-Enabled 112-Gb/s Transmission System," in *IEEE Photonics Journal*, vol. 7, no. 3, pp. 1-13, June 2015.

[10] D. Patel, S. Ghosh, M. Chagnon, A. Samani, V. Veerasubramanian, M. Osman, and D. Plant, "Design, analysis, and transmission system performance of a 41 GHz silicon photonic modulator," *Opt. Express* 23, 14263-14287 (2015).

[11] M. Chagnon, M. Morsy-Osman, M. Poulin, C. Paquet, S. Lessard and D. V. Plant, "Experimental Parametric Study of a Silicon Photonic Modulator Enabled 112-Gb/s PAM Transmission System With a DAC and ADC," in *Journal of Lightwave Technology*, vol. 33, no. 7, pp. 1380-1387, April1, 1 2015.

[12] X. Tu, T. Liow, J. Song, M. Yu, and G. Lo, "Fabrication of low loss and high speed silicon optical modulator using doping compensation method," *Opt. Express* **19**, 18029-18035 (2011).

[13] Ilya Goykhman, Boris Desiatov, Shalva Ben-Ezra, Joseph Shappir, and Uriel Levy, "Optimization of efficiency-loss figure of merit in carrier-depletion silicon Mach-Zehnder optical modulator," *Opt. Express 21*, 19518-19529 (2013).

[14] J. C. Rosenberg, W. M. J. Green, S. Assefa, D. M. Gill, T. Barwicz, M. Yang, S. M. Shank, and Y. A. Vlasov, "A 25 Gbps silicon microring modulator based on an interleaved junction," *Opt. Express 20*, 26411-26423 (2012).

[15] D. M. Gill, C. Xiong, J. C. Rosenberg, P. Pepeljugoski, J. S. Orcutt, and W. M. J. Green, "Modulator figure of merit for short reach data links," *Opt. Express* 25, 24326-24339 (2017)

[16] Nikolay A. Kaliteevskiy, William A. Wood, John D. Downie, Jason Hurley, Petr Sterlingov, "Power penalties for multi-level PAM modulation formats at arbitrary bit error rates," *Proc. SPIE 9775, Next-Generation Optical Networks for Data Centers and Short-Reach Links III*, 977508,7 March 2016.

[17] D. Gill, W. Green, S. Assefa, J. Rosenberg, T. Barwicz, S. Shank, H. Pan, and Y. Vlasov, "A figure of merit based transmitter link penalty calculation for CMOS-compatible plasma-dispersion electro-optic Mach–Zehnder modulators," arXiv:1211.2419 (2012).

[18] H. Bahrami, H. Sepehrian, C. S. Park, L. A. Rusch and W. Shi, "Time-Domain Large-Signal Modeling of Traveling-Wave Modulators on SOI," in Journal of Lightwave Technology, vol. 34, no. 11, pp. 2812- 2823, June1, 1 2016.

Hassan Sepehrian (S'08) received the B.S. degree from the Shahed University of Tehran, Tehran, Iran, in 2008 and his M.Sc. degree (with honors) from the Ferdowsi University of Mashhad, Mashhad, Iran, in 2010. He is currently working toward his Ph.D. degree at the Department of Electrical and Computer Engineering, the Center for Optics, Photonics and Lasers (COPL), Université Laval, Québec, QC, Canada. His research interests include Integrated Silicon Photonic electro-optic devices, integrated electro-optic transceivers, and mixed-signal integrated circuits.

Amin Yekani was born in Tabriz, Iran, in 1989. He received his B.S. degree in electrical engineering from the University of Tabriz, Tabriz, Iran, in 2011 and his M.S. degree in electrical engineering from the Centre for Optics Photonics, and Lasers (COPL), ECE department, Université Laval, QC, Canada, in 2015, where he is currently working toward his Ph.D. degree.

Mr. Yekani's current research interests include digital signal processing and advanced modulation formats for optical short reach interconnects and passive optical networks, especially on Silicon Photonics modulators.

Wei Shi (S'07–M'12) received the Ph.D. degree in electrical and computer engineering from the University of British Columbia,Vancouver, BC, Canada, in 2012. He is currently an Assistant Professor with the Department of Electrical and Computer Engineering, Université Laval, Québec, QC, Canada. During the Ph.D. degree, he received many awards and scholarships including the BCIC Innovation Scholarship. Before joining Université Laval in 2013, he was a Researcher at McGill University, Montreal, QC, where he held an NSERC Postdoctoral Fellowship. His research interests include silicon photonics and integrated electronic- photonic systems for high-capacity optical transmissions.

Leslie Ann Rusch (S'91-M'94-SM'00-F'10) received the B.S.E.E. degree (with honors) from the California Institute of Technology, Pasadena, in 1980 and the M.A. and Ph.D. degrees in electrical engineering from Princeton University, Princeton, NJ, in 1992 and 1994, respectively. She holds a Canada Research Chair in Communications Systems Enabling the Cloud, is a full professor in the ECE department at Université Laval, QC, Canada where she is also a member of the Centre for Optics, Photonics, and Lasers (COPL). Dr. Rusch has experience in defense, industrial and academic communications research. She was a communications project engineer for the Department of Defense from 1980-1990. While on leave from Université Laval, she spent two years (2001-2002) at Intel Labs creating and managing a group researching new wireless technologies.

Prof. Rusch performs research on wireless and optical communications. Her research interests include digital signal processing for coherent detection in optical communications, spatial multiplexing using orbital angular momentum

modes in fiber, radio over fiber and OFDM for passive optical networks; and in wireless communications, optimization of the optical/wireless interface in emerging cloud based computing networks, and implantable medical sensors with high bit rate UWB telemetry. She is recipient of the IEEE Canada J. M. Ham Award for Graduate Supervision. Prof. Rusch has published over 128 journal articles in international journals (90% IEEE/IEE) with wide readership, and contributed to over 165 conferences. Her articles have been cited over 4500 times per Google Scholar.

National Science and Engineering Research Council of Canada (NSERC) Funding: CRDPJ 486716-15